

Multiparametric and Multinuclear Magnetic Resonance Imaging of Human Breast Cancer: Current Applications

www.tcrt.org

The exploration of novel imaging methods that have the potential to improve specificity for the identification of malignancy is still critically needed in breast imaging. Changes in physiologic alterations of soft tissue water associated with breast cancer can be visualized by magnetic resonance (MR) imaging. However, it is unlikely that a single MR parameter can characterize the complexity of breast tissue. Techniques such as multiparametric MR imaging, proton magnetic resonance spectroscopic (MRSI) imaging, and ²³Na sodium MR imaging when used in combination provide a comprehensive data set with potentially more power to diagnose breast disease than any single measure alone. A combination of MR, MRSI, and ²³Na sodium MR parameters may be examined in a single MR imaging examination, potentially resulting in improved specificity for radiologic evaluation of malignancy.

Key words: Breast, Magnetic Resonance Imaging, Sodium MR, ²³Na, Spectroscopy, Proton, ISODATA, Cancer, Diffusion, Neoplasm.

Introduction and Review

Several factors have been identified that result in increased risk for the development of breast cancer, including hormonal status, reproductive history, age, diet, genetics predisposition, and sociodemographics (1-8).

Current treatment regimens for breast cancer are most effective when disease is detected at an early stage, at present these include prophylactic mastectomy, a radical approach that may be reserved for select women, or chemoprevention. While many agents are under investigation, only tamoxifen is approved by the FDA for reduction of risk of developing breast cancer. However, tamoxifen is prescribed for 5 years and prevents only hormone receptor positive tumors. Thus, it is likely that only women at very high risk for breast cancer may choose to take the treatment. Until better approaches for cancer prevention become available, the key to further improving survival is early detection and diagnosis. The most common methods used for the detection breast cancer in clinical practice are clinical breast exam (CBE), x-ray mammography, and ultrasound (6, 9-20).

Mammography is an effective tool for early screening and detection of breast cancer (6, 16-19). Despite the moderate to high sensitivity of mammography (70-90%) (21-23), the technique has limited specificity (32-64%) and mammography frequently cannot distinguish benign from malignant disease (19, 20, 24). Approximately 10% of cancers are not detected with mammography, often due to dense fibroglandular tissue that obscures visualization of the tumor (11, 14,

Michael A. Jacobs, Ph.D.^{1*}
Ronald Ouwerkerk, Ph.D.¹
Antonio C. Wolff, M.D.²
Vered Stearns, M.D.²
Paul A. Bottomley, Ph.D.¹
Peter B. Barker, D.Phil.^{1,4}
Pedram Argani, M.D.^{2,3}
Nagi Khouri, M.D.¹
Nancy E. Davidson, M.D.²
Zaver M. Bhujwalla, Ph.D.¹
David A. Bluemke, M.D., Ph.D.¹

¹The Russell H. Morgan Department of Radiology and Radiological Science

²Department of Oncology

³Department of Pathology

The Johns Hopkins University School of Medicine

Baltimore, MD 21205 USA

⁴F.M. Kirby Research Center for

Functional Brain Imaging

Kennedy Krieger Institute

Baltimore, MD 21205 USA

* Corresponding Author:
Michael A. Jacobs, Ph.D.
Email: mikej@mri.jhu.edu

15). The limitations in the sensitivity of mammography have led to the use of adjunctive imaging methods. For example, breast ultrasound (US) is used as an adjunct in the diagnostic evaluation of palpable masses and differentiation of cystic versus solid masses (13, 20, 25). However, US is highly user dependent with demonstrated intra- and inter-variability in the interpretation of breast sonograms (26).

MR imaging has shown promise for detection and characterization of breast lesions (14, 24, 27-33). Early studies of MR imaging of the breast using only T1 or T2 weighted images were disappointing (34-37), but gadolinium contrast enhanced MR has enabled substantial improvements in the method (38, 39). Contrast enhanced MR studies have reported high sensitivity (up to 100%); but variable specificity (~30-85%) (28, 29, 31, 38, 40-44) for breast cancer. The degree of enhancement, for example, of fibroadenomas may overlap with that of malignant lesions (45-47).

Assessing the enhancement of breast lesions by MR imaging has been refined by measuring time-intensity curves following the injection of the gadolinium contrast agent (44, 48, 49). Several distinct patterns of enhancement have been associated with benign versus malignant breast lesions (44, 49). The most commonly identified enhancement patterns have been defined as persistent, plateau, and washout patterns. Persistent enhancement is described by a monotonic increase of MR signal, plateau enhancement increases to a

constant level or “plateau”, and washout enhancement shows an initial peak followed by an immediate decrease in the signal intensity. Numerically, these patterns are referred to as type 1 (persistent), type 2 (plateau), or type 3 (washout). Type 1 enhancement has been shown to be suggestive of a benign lesion, whereas, type 3 enhancement is highly associated with breast malignancy (44). Type 2 enhancement can be seen in both benign and malignant lesions (44) and is thus equivocal; these breast lesions are managed as though they are malignant until proven otherwise.

In order to improve the specificity of breast MR imaging, several other approaches using diffusion- and perfusion-weighted imaging and/or contrast agents (50-52). Diffusion-weighted imaging (DWI) and perfusion (PWI) are sensitive to changes in the micro diffusion of water within the intra- and intercellular environments. These changes in the diffusion of water result in signal intensity changes on the DWI and/or PWI within the region of interest. The reason for these signal intensity changes on DWI are not exactly known; however, there is evidence that these changes may be attributable to many factors, such as shifts of water from the extracellular space to the intracellular space, increased tortuosity of the diffusion pathways, restriction of the cellular membrane permeability, cellular density, and disruption of cellular membrane depolarization (53-58). Moreover, DWI also provides a quantitative biophysical parameter, called the apparent diffusion coefficient of water (ADC). The ADC value is an indicator of the movement of water within the tissue. It gives an average value of the flow and distance a water molecule has moved (54). For example, a “decreased” ADC is interpreted as “reduced” flow of water,

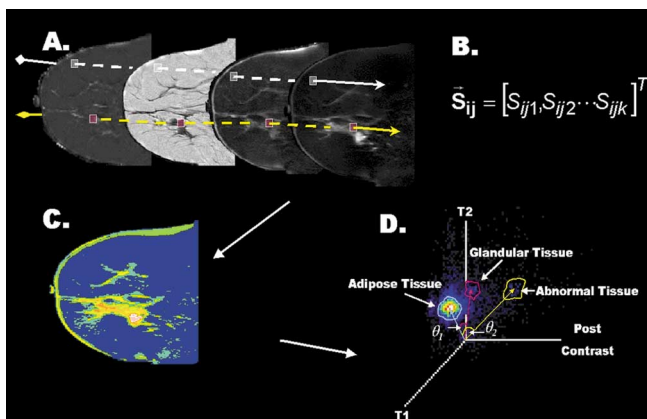


Figure 1: Demonstration of tissue signature vectors for different breast tissue types on MR data from a patient. **A)** Signature vectors are defined for each separate normal tissue type (adipose and glandular) and assigned to the cluster that closely resembles its vector elements in the ISODATA algorithm. **B)** The mathematical description of the tissue signature vector. **C)** A representative ISODATA theme map from the tissue signature vectors defined from each tissue cluster. **D)** Representation of the three-dimensional (3D) feature space formed by T1, fat sat T2, and post-contrast MR image (the 3D-feature space is shown for easy visualization). The angle separation model is demonstrated with the distribution of tissue clusters in 3D-feature space. Angles are calculated by the dot product between the normal tissue and abnormal tissue clusters using each cluster’s tissue signature vector as shown by θ_1 and θ_2 . Each axis represents the signal intensity distribution for each MR image. Adapted from (68).

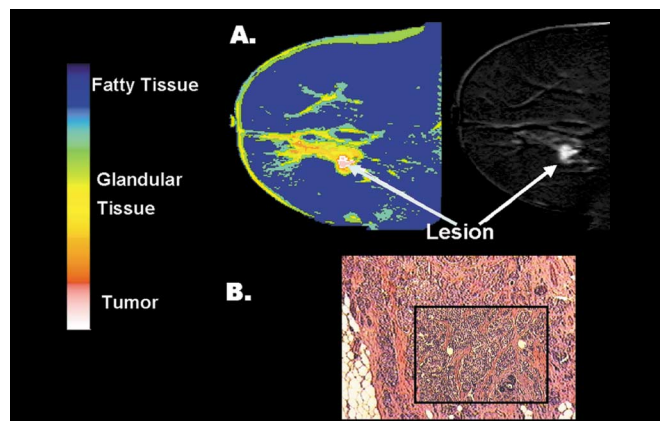


Figure 2: **A)** The ISODATA methodology and subtracted sagittal T1WI contrast weighted image from a 56-year-old woman with invasive ductal carcinoma confirmed by histology. The ISODATA segmentation demonstrates clear separation of different breast tissue types; fatty tissue (blue) from the glandular tissue (light green to yellow) versus the lesion (pink and white). **B)** Histological photomicrographs of magnified regions (2B-4 \times , insert-10 \times) were taken from the lesion area show invasive carcinoma. Adapted from (68).

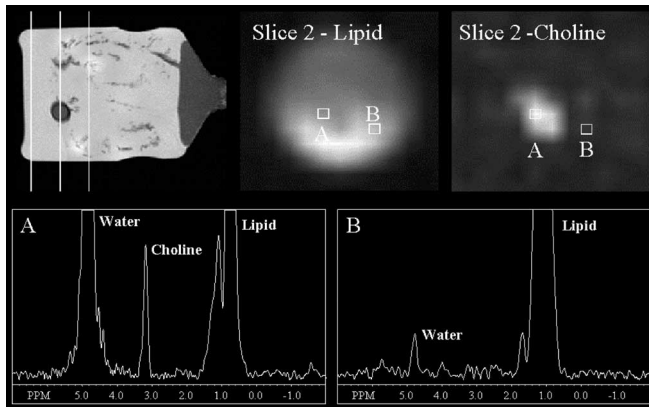


Figure 3: Phantom [10mM] demonstrating the proton MRSI methods. Lipid and choline maps are shown with respective spectra. **A)** Choline is present at 3.2 ppm within the “lesion”. **B)** Lack of choline signal in voxels outside the choline phantom.

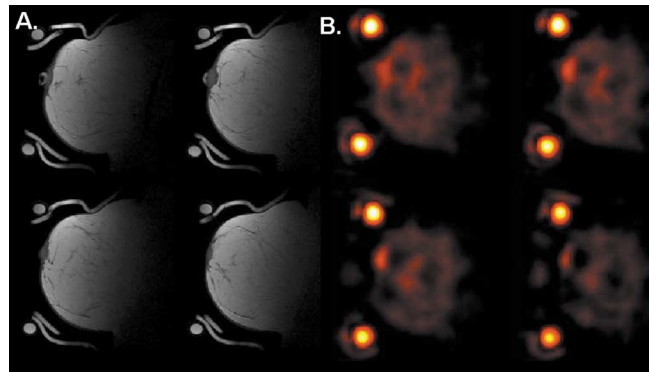


Figure 5: Two sets of corresponding sagittal breast MR images from a 33-year-old normal volunteer. **A)** T1 weighted images. **B)** Sodium MR images of the same location. The nipple is apparent within the Sodium Image colocalized with the TIWI. Bright objects in the sodium images external to the breast are reference phantoms.

whereas in tissue, an “increased” ADC indicates no restricted water flow. Clinical breast DWI studies have shown a distinction between malignant and benign tumors with a correlation between the cellularity and ADC value (50-52).

In addition, a novel three-time point (3TP) method has been explored using contrast agents (59). The 3TP method using the kinetics of the uptake within the lesion and can classify it as either benign or malignant. Also, MR spectroscopy (MRS) (60-66) and/or spectroscopic imaging (MRSI) (32) have been developed and applied with good success and will be further discussed below.

In another approach, we have developed and used characteristic tissue signature vectors derived from multiple different MR imaging pulse sequences (67,68). This multiparametric approach determines the angular separation between benign and malignant tissue signature vectors (68) based on MR signal on fat suppressed T2-weighted images (T2WI), T1-

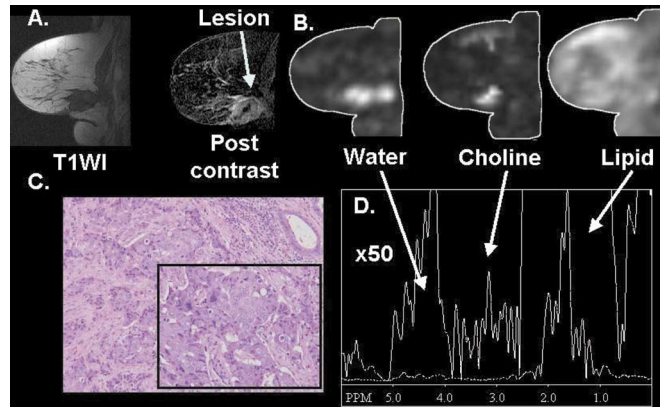


Figure 4: **A)** Sagittal T1-weighted MR and **B)** proton MRSI images in a 63 year old woman with invasive ductal carcinoma. **C)** Histological photomicrographs of magnified regions (2B-4x, insert-10x) were taken from the lesion area. **D)** Representative spectrum and magnified (x50) region demonstrate a detectable Cho signal (SNR=6.6) in the lesion at 3.2 ppm.

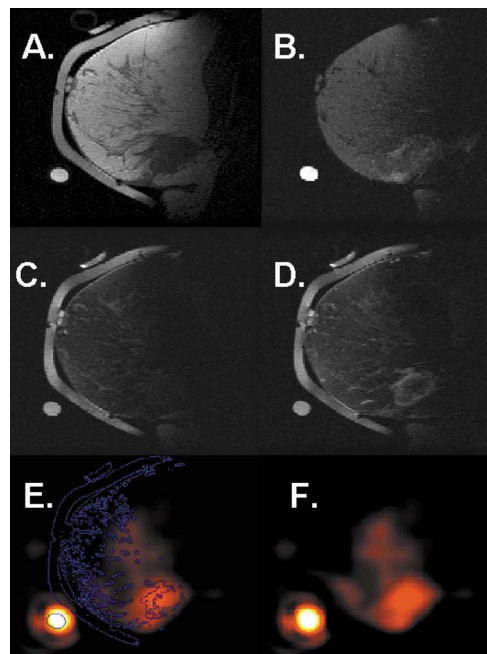


Figure 6: **A)** Sagittal T1 weighted image of a 63 year old woman with invasive carcinoma in the lower inner breast. **B)** Fat suppressed fast spin echo T2 weighted image. Fat suppressed T1-weighted Pre **(C)** and post **(D)** gadolinium contrast enhanced MR image. **E-F)** Sodium images demonstrating increased sodium signal within the breast lesion. Note, a blue contour plot generated on **(D)** is shown superimposed on the sodium image in **(E)**.

weighted images (T1WI), and fat suppressed T1WI before and after a gadolinium contrast agent is administered. In addition, sodium MR (^{23}Na) and proton (^1H) MRS data are available to help to resolve equivocal breast cases in the multiparametric model. The purpose of this report is to review data applicable to this tissue signature model for multiparametric breast MR imaging including ^{23}Na sodium and MRSI for extending breast cancer research.

Methods and Materials

Clinical Subjects

Female patients (n=59, age:18-80) were referred for MR evaluation of breast lesions identified by X-ray mammography, ultrasound, or clinical breast exam (palpable breast mass). Either core biopsy, excisional biopsies, lumpectomy, or mastectomy were performed. Lesions were considered benign if they showed specified fibrocystic changes, including formation of cysts, increased fibrous tissue, benign patterns of duct or lobule distortion, and benign cellular changes (typical or atypical lobular or ductal hyperplasia). Lesions with a histological diagnosis of ductal or invasive carcinoma were considered malignant. The protocol was approved by our Institutional Review Board, and informed consent was obtained from all subjects.

MR Imaging Protocol

Proton MR Imaging: MR imaging was performed on a 1.5 T MR scanner (General Electric Med. Sys.), using a dedicated phased array breast coil (Medrad,PA) with the patient in the prone position. MR sequences were: sagittal fat suppressed T2WI fast spin echo (TR/TE=5700/102) and fast spoiled gradient echo (FSPGR) T1WI (TR/TE =200/4.4) with field of view (FOV) = 18-20 × 18-20 cm (adjusted to the size of the breast), matrix = 256 × 192, slice thickness, 4 mm, 1mm gap). In addition, fat suppressed three dimensional FSPGR T1WI (TR/TE=20/4, matrix = 512 × 160, slice thickness, 2 mm) pre- and post-contrast images were obtained after intravenous administration of 0.1 mmol/kg gadodiamide contrast agent (Omniscan, General Electric Health Systems. The contrast agent was injected over 10 seconds with MR imaging beginning immediately after completion of the injection. The contrast bolus was immediately followed by a 20cc saline flush. Total scan time for the protocol was less than 20 minutes.

Proton Spectroscopy: Shimming was first performed to optimize field homogeneity. Water suppression was optimized using automated routines provided by the manufacturer using a three sequential "CHESS" pulses with a bandwidth of 75 Hz, applied on-resonance with the water signal (69). Lipid signals were attenuated by using an inversion pulse (STIR) with a delay of 171 msec. The MRSI section location was defined by a radiologist (DAB) to include the lesion. Proton MRSI was next performed on a single 10mm thick sagittal section using a point resolved spectroscopy sequence (PRESS) after the completion of proton contrast MR imaging. MRSI scan parameters were TR/TE 2000/272ms, 18 × 18 matrix size, 18cm FOV. The nominal voxel size was approximately 1.0cc. The echo signal was digitized with 256 data points and a spectral width of 1000 Hz. After MRSI, a set of double gradient-echo images (TR/TE 250/14,25ms) were recorded at the same slice loca-

tions in order to calculate maps of the B_0 magnetic field strength, and to ensure that the subject had not moved during the MRSI scan. Total scan time for the proton spectroscopy protocol was approximately 15 minutes.

23 Na Sodium MR: Sodium MRI was done with a Twisted Projection Imaging (TPI) sequence which allows ultra short TE (=0.4ms) as described previously (70, 71). A custom built 3-turn solenoid sodium coil was designed to fit in the phased array MR breast coil (Medrad,PA). Six signal averages were recorded for 718 projections at TR=120ms using a 400 microsecond adiabatic half passage pulse for a uniform 90 degree excitation. Transmit power was set to provide enough RF amplitude for adiabatic excitation at any coil load. A ring shaped phantom filled with a 150 mM sodium solution served as concentration reference. Total scan time for the entire protocol was approximately 12 minutes.

MR Image Preprocessing and Analysis

MR image analysis was performed using a SUN Ultra SPARC60 workstation (Sun Microsystems Inc., Mountain View, CA.) using the Eigentool image analysis software (Image Analysis Lab, Henry Ford Hospital, Detroit MI. (72, 73)). Removing (subimaging) the background from the image to better visualize the breast from was accomplished using thresholding and morphological operations (74). After subimaging, an inhomogeneity correction method was applied to the MR imaging data set.

MRSI data were reconstructed using in-house software (developed by PBB) on a Sun Ultra SPARC60 computer system (Sun Microsystems Inc., Mountain View, CA.). The MRSI data sets were processed by three-dimensional Fourier transformation, with cosine filtering in the spatial domains after zero-filling to a 32 × 32 matrix. Exponential line broadening of 3 Hz, zero-filling in the time domain to 2048 data points. Applying a high-pass convolution filter was also applied to remove the residual water signal (50 Hz stop-band) in the time-domain. After setting the chemical shift of water to 4.7 ppm, spectroscopic images were created by numerical integration over the following chemical shift ranges: 3.14 to 3.34 ppm for choline (Cho), 0 to 1.45 ppm for lipids, and 4.2-5.2 ppm for water. For display, metabolic images were linearly interpolated to 256 × 256 points. The peak height of the signal in the Cho frequency range in one voxel located completely within the lesion was quantified using a simplex curve-fitting routine and expressed as a ratio relative to the background noise level between 7.0 and 9.0 ppm (where no signals are expected) in the same voxel to determine a signal to noise ratio (SNR). The cut value for the SNR determining benign from malignant tissue was set at 4.0. The voxel size, and all MRSI parameters were the same for each subject (32).

The multiparametric ISODATA segmentation used the T1WI, T2WI, pre- and post-contrast T1 MR image data set to define tissue signature vectors described in (68). Tissue signature vectors of adipose and glandular tissue were defined from all the images within the data set. These tissue signature vectors set the normal tissue inputs for the ISODATA algorithm. Then, tissue classes were automatically determined by the ISODATA routine, which outputs a theme map representing the different clusters (Fig. 1). A radiologist visually verified the adipose tissue from the theme map by its appearance on T1 and T2 weighted images. The adipose tissue vector was further used as a reference vector for measuring the angular separation of the other clusters identified by ISODATA. Classifications of different tissue types were determined from the angular separation between each tissue signature vector (Fig 1). The angle was calculated using the dot product between the tissue signature vectors. The ISODATA model result for the lesion was compared with the histopathological findings.

Statistical Analysis

The differences in the angular separation, spectroscopy choline SNR, and ^{23}Na sodium concentrations of the benign and malignant groups were evaluated using a Student's *t*-test. Statistical significance was set at $p < 0.05$.

Results and Discussion

Proton MR

The multiparametric ISODATA model segmented normal from abnormal breast tissue and was also able to differentiate between adipose and glandular tissue types (68). Figure 2 demonstrates a representative multiparametric ISODATA segmentation from a 56-year-old patient with invasive ductal carcinoma. The ISODATA segmentation of adipose tissue (blue) from the glandular tissue (light green to yellow) is shown in Figure 2A. Representative histological images from the lesion are shown in Figure 2B. Overall, for malignant lesions ($n=20$), the average angular separation between adipose and tumor tissue was $17.5^\circ \pm 5.9^\circ$ (mean angle \pm standard deviation). For benign lesions ($n=20$) the average angular separation was $29.1^\circ \pm 10.6^\circ$ between adipose tissue and lesion tissue. The angular separation between malignant and benign lesions was significantly different ($p=0.005$). There was no demonstrable significant difference ($p=0.65$) between the glandular tissue signature vectors in patients with benign or malignant lesions. The result of our classification method is comparable to the ones achieved by other studies. For example, using an angular separation of 21° , a sensitivity of 89% and specificity of 78% was achieved. At higher angles, a sensitivity of 94% with specificity of 72% was realized. These data demonstrates the potential of the angular separa-

tion model to correctly identify and classify breast lesions. The advantage of the multiparametric method is that it can be extended to include other MR data sets such as MRSI and/or ^{23}Na Sodium. The incorporation these different types MR data will allow the integration of "molecular" with "diagnostic" data. This will enable our team to investigate both of these important parameters with normal/abnormal "diagnostic" parameters. Therefore, the ISODATA results will provide, for the first time, a combined "tissue-molecular map" of each different breast tissue vector. The goal of subsequent multiparametric analysis will be to determine the minimum number of parameters that objectively and quantitatively yield optimum sensitivity and specificity.

MRSI: Figures 3 and 4 demonstrate representative MR and MRSI images and spectra on a phantom and patients with breast cancer. Choline (Cho) is visible in the phantom measurements [10mM] as shown in Figure 3. This demonstrates that proton spectroscopy can detect Cho. Figure 4 shows a 63-year-old patient with an infiltrating ductal carcinoma (Fig 4C). Elevated choline (Fig 4D) is apparent within the MRSI image and spectra, co-localized with the contrast-enhanced T1WI. The distribution of water and lipid on MRSI also corresponds to the expected distribution seen on MRI (*i.e.*, lipid from adipose tissue, water from the lesion and ductal tissue). We have found a significant ($p < 0.0008$) difference between the Cho SNR for benign and malignant patients ($n=15$) (32).

We decided to use the Cho SNR ratio as an objective measure of the magnitude of the Cho signal. We recognize that the SNR depends on several technical factors (75), such as the receiver coil quality (Q) factor. The Q factor can vary from subject to subject due to different coil loading factors. In theory, this different loading may be corrected by measuring the power required for a 90 degree pulse, but for breast MR usually the body coil is used for transmitting RF pulses, and it is unlikely that the body transmit and surface receive coils are equally loaded. Therefore, while measuring SNR gave us an approximate index of lesion Cho levels and indicated them to be higher in malignant than benign lesions, improved methods for the quantitation of Cho in breast lesions are needed. Currently, different strategies exist for quantitation of MRSI of the brain (76-80) and it appears likely that these methods may be adapted for the breast (81), although there are significant differences between brain and breast MRSI (*e.g.*, different RF coils used (volume vs. surface)), different tissue types (*i.e.*, no "reference" metabolites (such as Cr) in breast)). Several prior breast MRSI studies have simply rated lesion spectra for the presence or absence of Cho. However, this method is in general problematic, since clear criteria need to be established for when a signal is "detectable" or not, and in addition changes to the system (*e.g.*, field strength, detection coils, etc) or protocol (*e.g.*, pulse sequence, voxel size, scan time) will alter the SNR and

hence the threshold at which Cho would become detectable. Therefore, we selected a conservative estimate of SNR=4 to determine if the lesion was benign or malignant. Also, by the addition of spectroscopy to a dynamic gadolinium MR imaging breast examination may increase the specificity of the diagnosis of malignancy (33, 66).

²³Na Sodium: Sodium imaging assesses different tissue characteristics than either the proton or MRSI exam by reflecting alterations in the cell ionic status or membrane permeability. For example, elevated sodium levels are associated with disruption of the membrane sodium-potassium pump and changes in the water environment within breast tissue. Figure 5 demonstrates representative T1WI and sodium MR images on a volunteer. Volunteers (n=5) had no focal elevations of sodium within breast tissue. In patients with diagnosed breast cancer (n=4), mean lesion size was 4.4 ± 2.3 cm. Breast lesions were hyperintense on sodium images (Figure 6). Mean ²³Na MRI determined sodium concentration for fatty tissue was 20 ± 2 mM/kg, 28 ± 4 mM/kg in glandular tissue, and 47 ± 12 mM/kg in breast cancers. All cancers demonstrated significantly ($p < 0.005$) increased sodium content compared to glandular and fatty tissue.

In conclusion, we have demonstrated that molecular and metabolic breast MR imaging is feasible in the clinical setting. These methods provide a basis for a comprehensive interrogation of the complex tumor environment. Spectroscopy demonstrates the presence of choline, which has been associated with malignancy (33, 60, 61, 65, 82).

Thus, by using a combination of different MR parameters we may be able to develop a more complete "model" in diagnosing breast cancer noninvasively. These initial studies demonstrate that both proton and ²³Na sodium MR may provide additional information that may assist with the MR diagnosis of breast cancer or that may be useful in monitoring therapeutic interventions (83-85). Further studies are needed to expand the use of these novel methods to become "routine" diagnostic exams.

Acknowledgements

We thank the assistance of Cindy Maranto and Cheryl Arnold in obtaining the MR data and Lucie Bower, Dr Donald Peck, and Dr. Hamid Soltanian-Zadeh, Henry Ford Hospital, Detroit, MI for the Eigentool image analysis software used for image processing. This work was supported in part by NIH 1R01CA100184 (MAJ), P50 CA103175 (MAJ/ZAB), NIH Breast Spore CA88843 (PA, ACW, VS, NED), R21CA-95907(RO) RO1-HL61695 (PAB) and 1R21CA/RR91798-01 (PBB).

References

1. Wooster, R., Bignell, G., Lancaster, J., *et al.* Identification of the Breast-Cancer Susceptibility Gene Brca2. *Nature* 378, 789-792 (1995).
2. Wooster, R., Neuhausen, S. L., Mangion, J., *et al.* Localization of a Breast-Cancer Susceptibility Gene, Brca2, to Chromosome 13q12-13. *Science* 265, 2088-2090 (1994).
3. Chappuis, P. O., Nethercot, V., and Foulkes, W. D. Clinico-pathological Characteristics of BRCA1-and BRCA2-related Breast Cancer. *Seminars in Surgical Oncology* 18, 287-295 (2000).
4. Cox, L. A., Chen, G., and Lee, E. Tumor-Suppressor Genes and Their Roles in Breast-Cancer. *Breast Cancer Research and Treatment* 32, 19-38 (1994).
5. Miki, Y., Swensen, J., Shattuckeids, D., *et al.* A Strong Candidate For the Breast and Ovarian-Cancer Susceptibility Gene Brca1. *Science* 266, 66-71 (1994).
6. Vogel, V.G. Breast Cancer Prevention: A Review of Current Evidence. *CA Cancer J. Clin.* 50, 156-170 (2000).
7. McPherson, K., Steel, C. M., and Dixon, J. M. ABC of Breast Diseases – Breast-Cancer – Epidemiology, Risk-Factors, and Genetics. *British Medical Journal* 309, 1003-1006 (1994).
8. Richardson, J. L., Langholz, B., Bernstein, L., Burciaga, C., Danley, K., and Ross, R. K. Stage and Delay in Breast Cancer Diagnosis by Race, Socioeconomic Status, Age and Year. *Br. J. Cancer* 65, 922-926 (1992).
9. Umschaden, H. W. and Haselbach, H. MR-Mammography: State of the Art and Indications. *Acta. Medica. Austriaca.* 24, 39-45 (1997).
10. Gilbert, F. J. New Screening Techniques for Breast Cancer (MRI). *Disease Markers* 15, 115-116 (1999).
11. Lawrence, W. F., Liang, W., Mandelblatt, J. S., *et al.* Serendipity in Diagnostic Imaging: Magnetic Resonance Imaging of the Breast. *J. Natl. Cancer Inst.* 90, 1792-1800 (1998).
12. Weinreb, J. C. and Newstead, G. MR-Imaging of the Breast. *Radiology* 196, 593-610 (1995).
13. Berg, W. A. and Gilbreath, P. L. Multicentric and Multifocal Cancer: Whole-breast US in Preoperative Evaluation. *Radiology* 214, 59-66 (2000).
14. Brauning, M. P. and Pisano, E. D. New Modalities in Breast Imaging: Digital Mammography and Magnetic Resonance Imaging. *Breast Cancer Res Treat* 35, 31-38 (1995).
15. Hardy, J. R., Powles, T. J., Judson, I., *et al.* How Many Tests are Required in the Diagnosis of Palpable Breast Abnormalities? *Clin Oncol (R Coll Radiol)* 2, 148-152 (1990).
16. Smith, R. A., Mettlin, C. J., Davis, K. J., and Eyre, H. American Cancer Society Guidelines for the Early Detection of Cancer. *CA Cancer J Clin* 50, 34-49 (2000).
17. Harris, K. M. and Vogel, V. G. Breast Cancer Screening. *Cancer and Metastasis Reviews* 16, 231-262 (1997).
18. Kaiser, W. A. MR Mammography. *MedicaMundi* 36, 168-82 (1991).
19. Feig, S. A. Decreased Breast Cancer Mortality through Mammographic Screening: Results of Clinical Trials. *Radiology* 167, 659-665 (1988).
20. Fischer, U., Kopka, L., and Grabbe, E. Breast Carcinoma: Effect of Preoperative Contrast-enhanced MR Imaging on the Therapeutic Approach. *Radiology* 213, 881-88 (1999).
21. Rosenberg, R. D., Hunt, W. C., Williamson, M. R., *et al.* Effects of Age, Breast Density, Ethnicity, and Estrogen Replacement Therapy on Screening Mammographic Sensitivity and Cancer Stage at Diagnosis: Review of 183,134 Screening Mammograms in Albuquerque, New Mexico. *Radiology* 209, 511-518 (1998).
22. Poplack, S. P., Tosteson, A. N., Grove, M. R., Wells, W. A., and Carney, P. A. Mammography in 53,803 Women from the New Hampshire Mammography Network. *Radiology* 217, 832-840 (2000).

23. Mandelson, M. T., Oestreicher, N., Porter, P. L., *et al.* Breast Density as a Predictor of Mammographic Detection: Comparison of Interval- and Screen-detected Cancers. *J. Natl. Cancer. Inst.* 92, 1081-1087 (2000).
24. KacI, G. M., Liu, P., Debatin, J. F., Garzoli, E., Caduff, R. F., and Krestin, G. P. Detection of Breast Cancer with Conventional Mammography and Contrast-enhanced MR Imaging. *Eur. Radiol.* 8, 194-200 (1998).
25. Stavros, A. T., Thickman, D., Rapp, C. L., Dennis, M. A., Parker, S. H., and Sisney, G. A. Solid Breast Nodules: Use of Sonography to Distinguish Between Benign and Malignant Lesions. *Radiology* 196, 123-134 (1995).
26. Baker, J. A. and Soo, M. S. Breast US: Assessment of Technical Quality and Image Interpretation. *Radiology* 223, 229-238 (2002).
27. Heywang, S. H., Wolf, A., Pruss, E., Hilbertz, T., Eiermann, W., and Permanetter, W. MR Imaging of the Breast with Gd-DTPA: Use and Limitations. *Radiology* 171, 95-103 (1989).
28. Orel, S. G., Schnall, M. D., Powell, C. M., *et al.* Staging of Suspected Breast-Cancer – Effect of MR-Imaging and MR-Guided Biopsy. *Radiology* 196, 115-122 (1995).
29. Orel, S. G. High-resolution MR Imaging for the Detection, Diagnosis, and Staging of Breast Cancer. *Radiographics* 18, 903-912 (1998).
30. Orel, S. G. and Schnall, M. D. MR Imaging of the Breast for the Detection, Diagnosis, and Staging of Breast Cancer. *Radiology* 220, 13-30 (2001).
31. Kriege, M., Brekelmans, C. T., Boetes, C., *et al.* Efficacy of MRI and Mammography for Breast-Cancer Screening in Women with a Familial or Genetic Predisposition. *N. Engl. J. Med.* 351, 427-437 (2004).
32. Jacobs, M. A., Barker, P. B., Bottomley, P. A., Bhujwala, Z., Bluemke, D. B. Proton MR Spectroscopic Imaging of Human Breast Cancer: A Preliminary Study. *J. Magn. Reson. Imaging* 19, 68-75 (2004).
33. Jacobs, M. A., Barker, P. B., Argani, P., Ouwerkerk, R., Bhujwala, Z. M., and Bluemke, D. B. Combined Dynamic Contrast and Spectroscopic Imaging of Human Breast Cancer. *J. Magn. Reson. Imaging* XX, in press (2005).
34. Heywang, S. H., Bassermann, R., Fenzl, G., *et al.* MRI of the Breast – Histopathologic Correlation. *Eur. J. Radiol.* 7, 175-182 (1987).
35. Adams, A. H., Brookeman, J. R., Merickel, M. B. Breast Lesion Discrimination Using Statistical Analysis and Shape Measures on Magnetic Resonance Imagery. *Comput Med Imaging Graph* 15, 339-349 (1991).
36. Kerslake, R. W., Carleton, P. J., Fox, J. N., *et al.* Dynamic Gradient-echo and Fat-suppressed Spin-echo Contrast-enhanced MRI of the Breast. *Clin. Radiol.* 50, 440-454 (1995).
37. Kuhl, C. K., Klaschik, S., Mielcarek, P., Gieseke, J., Wardelmann, E., and Schild, H. H. Do T2-weighted Pulse Sequences Help with the Differential Diagnosis of Enhancing Lesions in Dynamic Breast MRI? *J. Magn. Reson. Imaging* 9, 187-196 (1999).
38. Heywang, S. H., Hahn, D., Schmidt, H., *et al.* MR Imaging of the Breast Using Gadolinium-DTPA. *J. Comput. Assist. Tomogr.* 10, 199-204 (1986).
39. Kaiser, W. A. and Zeitler, E. MR Imaging of the Breast: Fast Imaging Sequences With and Without Gd-DTPA. Preliminary Observations. *Radiology* 170, 681-686 (1989).
40. Gilles, R., Guinebretiere, J. M., Shapeero, L. G., *et al.* Assessment of Breast Cancer Recurrence with Contrast-enhanced Subtraction MR Imaging: Preliminary Results in 26 Patients. *Radiology* 188, 473-478 (1993).
41. Harms, S. E., Flamig, D. P., Hesley, K. L., *et al.* MR Imaging of the Breast with Rotating Delivery of Excitation Off-resonance: Clinical Experience with Pathological Correlation. *Radiology* 187, 493-501 (1993).
42. Kelcz, F. and Santyr, G. Gadolinium-enhanced Breast MRI. *Crit. Rev. Diagn. Imaging* 36, 287-338 (1995).
43. Heywang-Kobrunner, S. H., Viehweg, P., Heinig, A., Kuchler, C. Contrast-enhanced MRI of the Breast: Accuracy, Value, Controversies, Solutions. *Eur. J. Radiol.* 24, 94-108 (1997).
44. Kuhl, C. K., Mielcarek, P., Klaschik, S., *et al.* Dynamic Breast MR Imaging: Are Signal Intensity Time Course Data Useful for Differential Diagnosis of Enhancing Lesions? *Radiology* 211, 101-110 (1999).
45. Heywang-Kobrunner, S. H., Haustein, J., Pohl, C., *et al.* Contrast-enhanced MR Imaging of the Breast: Comparison of Two Different Doses of Gadopentetate Dimeglumine. *Radiology* 191, 639-646 (1994).
46. Gribbestad, I. S., Nilsen, G., Fjosne, H. E., Kvinnsland, S., Haugen, O. A., Rinck, P. A. Comparative Signal Intensity Measurements in Dynamic Gadolinium-enhanced MR Mammography. *J. Magn. Reson. Imaging* 4, 477-480 (1994).
47. Orel, S. G., Schnall, M. D., LiVolsi, V. A., and Troupin, R. H. Suspicious Breast Lesions: MR Imaging with Radiologic-pathologic Correlation. *Radiology* 190, 485-93 (1994).
48. Boetes, C., Barentsz, J. O., Mus, R. D., *et al.* MR Characterization of Suspicious Breast Lesions with a Gadolinium-enhanced TurboFLASH Subtraction Technique. *Radiology* 193, 777-781 (1994).
49. Orel, S. G. Differentiating Benign from Malignant Enhancing Lesions Identified at MR Imaging of the Breast: Are Time-signal Intensity Curves an Accurate Predictor? *Radiology* 211, 5-7 (1999).
50. Sinha, S. and Sinha, U. Functional Magnetic Resonance of Human Breast Tumors: Diffusion and Perfusion Imaging. *Ann. NY Acad. Sci.* 980, 95-115 (2002).
51. Guo, Y., Cai, Y. Q., Cai, Z. L., *et al.* Differentiation of Clinically Benign and Malignant Breast Lesions Using Diffusion-weighted Imaging. *J. Magn. Reson. Imaging* 16, 172-178 (2002).
52. Sinha, S., Lucas-Quesada, F. A., Sinha, U., DeBruhl, N., and Bassett, L. W. *In Vivo* Diffusion-weighted MRI of the Breast: Potential for Lesion Characterization. *J. Magn. Reson. Imaging* 15, 693-704 (2002).
53. Moseley, M. E., Kucharczyk, J., Mintorovitch, J., *et al.* Diffusion-weighted MR Imaging of Acute Stroke: Correlation with T2-weighted and Magnetic Susceptibility-enhanced MR Imaging in Cats. *American Journal of Neuroradiology* 11, 423-429 (1990).
54. Le Bihan, D., Breton, E., Lallemand, D., Grenier, P., Cabanis, E., and Laval Jeantet, M. MR Imaging of Intravoxel Incoherent Motions: Application to Diffusion and Perfusion in Neurologic Disorders. *Radiology* 161, 401-407 (1986).
55. Benveniste, H., Hedlund, L., and Johnson, G. Mechanism of Detection of Acute Cerebral Ischemia in Rats by Diffusion-weighted Magnetic Resonance Microscopy. *Stroke* 23, 746-754 (1992).
56. Minematsu, K., Li, L., Fisher, M., Sotak, C. H., Davis, M. A., and Fiandaca, M. S. Diffusion Weighted Magnetic Resonance Imaging: Rapid and Quantitative Detection of Focal Brain Ischemia. *Neurology* 42, 235-240 (1992).
57. Hoehn-Berlage, M., Norris, D., Kohno, K., Mies, G., Leibfritz, D., and Hossmann, K. Evolution of Regional Changes in Apparent Diffusion Coefficient During Focal Ischemia of Rat Brain: The Relationship of Quantitative Diffusion NMR Imaging to Reduction in Cerebral Blood Flow and Metabolic Disturbances. *Journal of Cerebral Blood Flow & Metabolism* 15, 1002-1011 (1995).
58. Liu, K. F., Li, F., Tatlisumak, T., *et al.* Regional Variations in the Apparent Diffusion Coefficient and the Intracellular Distribution of Water in Rat Brain During Acute Focal Ischemia. *Stroke* 32, 1897-1905 (2001).
59. Degani, H., Gusic, V., Weinstein, D., Fields, S., and Strano, S. Mapping Pathophysiological Features of Breast Tumors by MRI at High Spatial Resolution. *Nat. Med.* 3, 780-782 (1997).

60. Roebuck, J. R., Cecil, K. M., Schnell, M. D., Lenkinski, R. E. Human Breast Lesions: Characterization with Proton MR Spectroscopy. *Radiology* 209, 269-275 (1998).
61. Kvistad, K. A., Bakken, I. J., Gribbestad, I. S., et al. Characterization of Neoplastic and Normal Human Breast Tissues with *In Vivo* (1)H MR Spectroscopy. *J. Magn. Reson. Imaging* 10, 159-164 (1999).
62. Cecil, K. M., Schnell, M. D., Siegelman, E. S., and Lenkinski, R. E. The Evaluation of Human Breast Lesions with Magnetic Resonance Imaging and Proton Magnetic Resonance Spectroscopy. *Breast Cancer Res. Treat* 68, 45-54 (2001).
63. Yeung, D. K., Cheung, H. S., and Tse, G. M. Human Breast Lesions: Characterization with Contrast-enhanced *In Vivo* Proton MR Spectroscopy – Initial Results. *Radiology* 220, 40-46 (2001).
64. Katz-Brull, R., Lavin, P. T., and Lenkinski, R. E. Clinical Utility of Proton Magnetic Resonance Spectroscopy in Characterizing Breast Lesions. *J. Natl. Cancer Inst.* 94, 1197-1203 (2002).
65. Kim, J. K., Park, S. H., Lee, H. M., et al. *In Vivo* 1H-MRS Evaluation of Malignant and Benign Breast Diseases. *Breast* 12, 179-182 (2003).
66. Huang, W., Fisher, P. R., Dulaimy, K., Tudorica, L. A., O’Hea, B., Button, T. M. Detection of Breast Malignancy: Diagnostic MR Protocol for Improved Specificity. *Radiology* 232, 585-591 (2004). [Epub Jun 17, 2004].
67. Jacobs, M. A., Bluemke, D. B., Bhujwala, Z., Marano, C., and Barker, P. B. A Model to Differentiate Benign From Malignant Breast Tumors using Multiparametric MRI with Histological Correlates. *Proceedings of the International Society of Magnetic Resonance 9th Scientific Meeting, 18th Annual Meeting, Glasgow, Scotland UK* 9, 563 (2001).
68. Jacobs, M. A., Barker, P. B., Bluemke, D. A., et al. Benign and Malignant Breast Lesions: Diagnosis with Multiparametric MR Imaging. *Radiology* 229, 225-232 (2003).
69. Haase, A., Frahm, J., Hancic, W., and Matthaei, D. H-1-Nmr Chemical-Shift Selective (Chess) Imaging. *Physics in Medicine and Biology* 30, 341-344 (1985).
70. Boada, F. E., Gillen, J. S., Shen, G. X., Chang, S. Y., and Thulborn, K. R. Fast Three Dimensional Sodium Imaging. *Magn. Reson. Med.* 37, 706-715 (1997).
71. Ouwerkerk, R., Bleich, K. B., Gillen, J. S., Pomper, M. G., and Bottomley, P. A. Tissue Sodium Concentration in Human Brain Tumors as Measured with ²³Na MR Imaging. *Radiology* 227, 529-537 (2003).
72. Jacobs, M. A., Knight, R. A., Windham, J. P., et al. Identification of Cerebral Ischemic Lesions in Rat Using Eigenimage Filtered Magnetic Resonance Imaging. *Brain Research* 837, 83-94 (1999).
73. Windham, J. P., Abd-Allah, M. A., Reimann, D. A., Froelich, J. W., and Haggar, A. M. Eigenimage Filtering in MR Imaging. *J Comput Assist Tomogr* 12, 1-9 (1988).
74. Jacobs, M. A., Knight, R. A., Soltanian-Zadeth, H., et al. Unsupervised Segmentation of Multiparameter MRI in Experimental Cerebral Ischemia with Comparison to T2, Diffusion, and ADC MRI Parameters and Histopathological Validation. *J. Magn. Reson. Imaging* 11, 425-437 (2000).
75. Soher, B. J., Hurd, R. E., Sailasuta, N., and Barker, P. B. Quantitation of Automated Single-voxel Proton MRS Using Cerebral Water as an Internal Reference. *Magn. Reson. Med.* 36, 335-339 (1996).
76. Pan, J. W., Twieg, D. B., and Hetherington, H. P. Quantitative Spectroscopic Imaging of the Human Brain. *Magn. Reson. Med.* 40, 363-369 (1998).
77. Michaelis, T., Merboldt, K. D., Bruhn, H., Hancic, W., and Frahm, J. Absolute Concentrations of Metabolites in the Adult Human Brain *In Vivo*: Quantification of Localized Proton MR Spectra. *Radiology* 187, 219-227 (1993).
78. Kreis, R., Ernst, T., and Ross, B. Absolute Quantitation of Water and Metabolites in the Human Brain II. Metabolite Concentrations. *J. Magn. Reson. B* 102, 9-19 (1993).
79. Barker, P. B., Soher, B. J., Blackband, S. J., Chatham, J. C., Mathews, V. P., and Bryan, R. N. Quantitation of Proton NMR Spectra of the Human Brain Using Tissue Water as an Internal Concentration Reference. *NMR Biomed* 6, 89-94 (1993).
80. Alger, J. R., Symko, S. C., Bizzi, A., Posse, S., DesPres, D. J., and Armstrong, M. R. Absolute Quantitation of Short TE Brain 1H-MR Spectra and Spectroscopic Imaging Data. *J. Comput. Assist. Tomogr.* 17, 191-199 (1993).
81. Bakken, I. J., Gribbestad, I. S., Singstad, T. E., and Kvistad, K. A. External Standard Method for the *In Vivo* Quantification of Choline-containing Compounds in Breast Tumors by Proton MR Spectroscopy at 1.5 Tesla. *Magn. Reson. Med.* 46, 189-192 (2001).
82. Jagannathan, N. R., Kumar, M., Raghunathan, P., Coshic, O., Julka, P. K., and Rath, G. K. Assessment of the Therapeutic Response of Human Breast Carcinoma using *In Vivo* Volume Localized Proton Magnetic Resonance Spectroscopy. *Current Science* 76, 777-782 (1999).
83. Delille, J.-P., Slanetz, P. J., Yeh, E. D., Halpern, E. F., Kopans, D. B., and Garrido, L. Invasive Ductal Breast Carcinoma Response to Neoadjuvant Chemotherapy: Noninvasive Monitoring with Functional MR Imaging – Pilot Study. *Radiology* 228, 63-69 (2003).
84. Jacobs, M. A., Ouwerkerk, R., Bottomley, P. A., et al. Multiparameter Proton, Sodium, and Spectroscopic Imaging of Human Breast Cancer. *Proceedings of the International Society of Magnetic Resonance 2003; 11th Scientific Meeting, 20th Annual Meeting, Toronto, Canada* 2003.
85. Meisamy, S., Bolan, P. J., Baker, E. H., et al. Neoadjuvant Chemotherapy of Locally Advanced Breast Cancer: Predicting Response with *In Vivo* 1H MR Spectroscopy – A Pilot Study at 4 T. *Radiology* 233, 424-431 (2004).

Date Received: October 29, 2004